Direct observation of bosonic quantum interference of surface plasmon polaritons using photon-number-resolving detectors

Go Fujii,[1,2,*] Daiji Fukuda,[2] and Shuichiro Inoue[1]

[1]*Institute of Quantum Science, Nihon University, 1-8-14 Kanda-Surugadai, Chiyoda-ku, Tokyo 101-8308, Japan*

[2]*National Institute of Advanced Industrial Science and Technology, 1-1-1 Umezono, Tsukuba-shi, Ibaraki 305-8568, Japan*

(Received 23 March 2014; revised manuscript received 2 August 2014; published 25 August 2014)

Quantum plasmonics is a field of research combining plasmonics with quantum optics and investigates interactions between photons and metallic nanostructures. So far, it has been proven that quantum properties of single photons to excite single surface plasmon polaritons (SPPs) are preserved in the process of photon-SPP-photon mode conversion in plasmonic nanostructures, which suggests the potential application of SPPs to the quantum information processing (QIP). Recently the Hong-Ou-Mandel (HOM) interference of single SPPs was observed in a plasmonic circuitry. However, the visibility was below the classical limit (50%) due to the simultaneous excitation of distinguishable SPP modes. We employed a directional coupler based on long-range surface-plasmon-polariton waveguides (LRSPP-DC) and superconducting photon-number-resolving detectors to directly observe the bosonic quantum interference of single SPPs beyond the classical limit. In addition, we demonstrated the indistinguishability of photons that excite single SPPs is well preserved in the process of photon-SPP mode conversion.

DOI: 10.1103/PhysRevB.90.085430 PACS number(s): 73.20.Mf, 42.50.−p, 85.25.−j, 03.67.−a

I. INTRODUCTION

SPPs are highly confined electromagnetic excitations coupled to the electron charge density waves propagating along a metal-dielectric interface. Significant efforts are currently devoted to the studies of their fundamental properties and their applications that take advantage of the subwavelength field confinement [1] and the electric-field enhancement [2]. In particular, an efficient coupling of single photons emitted from a single quantum dot [3] or a single nitrogen-vacancy center in diamond [4] to a metallic nanowire has attracted the interest of researchers in the field of quantum information science because of its potential application to a single-photon emitter [5]. In addition, optical quantum states have been preserved in the process of photon-SPP-photon mode conversion using plasmonic nanostructures [6–8]. These results suggest the feasibility of a plasmonic circuitry with single-SPP sources for the QIP. In such a circuitry, the quantum interference of single SPPs plays a central role to conduct the QIP.

The quantum interference of single photons has been demonstrated using the HOM interferometer [9]. Recently, the HOM interference of SPPs was demonstrated in a plasmonic circuitry consisting of an on-chip plasmonic beam splitter with integrated superconducting single photon detectors [10]. However, the visibility of the HOM interference was below the classical limit (50%). In the plasmonic circuitry, both of the short-range and long-range SPPs (LRSPPs) were excited, which causes the interference of not only indistinguishable single SPPs but also distinguishable single SPPs and results in the visibility that can be achieved using SPPs excited via weak coherent pulses [11].

We employed the LRSPP-DC [12] with total length of approximately 5 mm to perform the HOM interference experiment. Since the distance from the input port to the interaction region of the LRSPP-DC was approximately 100 times longer than the propagation length of the short-range SPPs, we were able to observe the quantum interference of single long-range SPPs beyond the classical limit. In addition, we directly observed the bosonic quantum interference of single long-range SPPs using photon-number-resolving detectors [13].

II. DIRECTIONAL COUPLER BASED ON LONG-RANGE SURFACE-PLASMON-POLARITON WAVEGUIDES

The LRSPP-DC is depicted in Fig. 1(a). To achieve a high coupling efficiency between the long-range surface-plasmon-polariton waveguide (LRSPP-WG) and an optical fiber, a low propagation loss, and single-mode propagation, our LRSPP-WGs consist of 20-nm-thin and 8-μm-wide gold stripes sandwiched between 22-μm-thick upper and lower cladding layers of polymer ZPU12-450 [14,15]. The LRSPP-DC has an interaction length of 500 μm and there is no gap between the coupled waveguides to achieve an output ratio of 50:50 [16]. To connect optical fibers to all input and output ports of the LRSPP-DC, each port was separated by 200 μm. To reduce the bending loss, the bend radius was designed to be 12 mm [17]. Accordingly, the total length of the LRSPP-DC was 5 mm. Figure 1(b) shows a microscope image of the fabricated LRSPP-DC. The LRSPP stripe mode was excited via end-fire coupling of photons polarized perpendicular to the waveguide surface by aligning a cleaved fiber facet with the end of a stripe [18]. Figure 1(c) shows the far-field image of the LRSPP-DC outputs when laser light is injected into one of the input ports. The two bright spots were observed, which indicates that the LRSPP-DC well works as a power splitter of LRSPPs. We then confirmed that the excited LRSPPs are in a single spatial mode. The insertion loss was approximately 30 dB. The output ratio is defined by R/T, where R is the reflectivity and T is the transmissivity. The measured output ratio was 61/39. Here we assumed that the coupling efficiencies at each port and the propagation losses of each waveguide were the same. The difference between the designed output ratio and the measured

*go-fujii@aist.go.jp

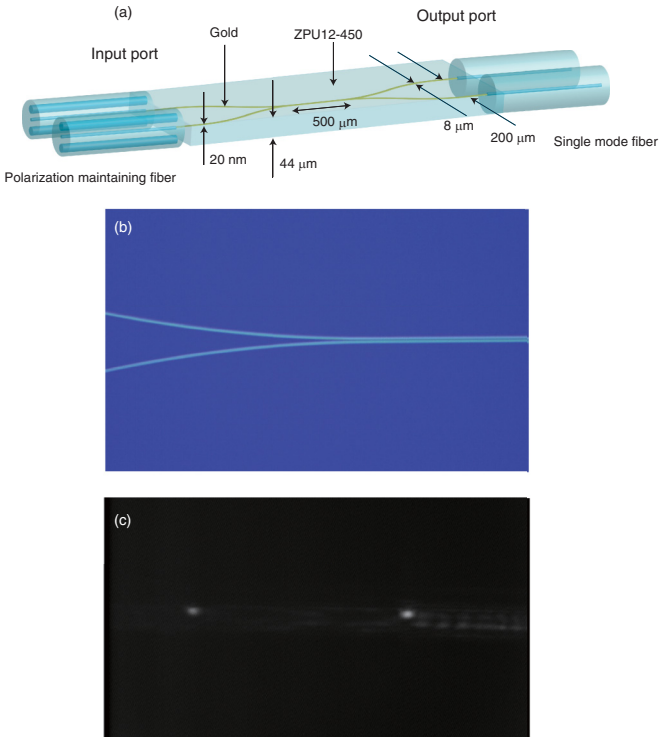

FIG. 1. (Color online) (a) Schematic of the LRSPP-DC. (b) Microscope image of the fabricated device. (c) The far field image of the LRSPP-DC outputs.

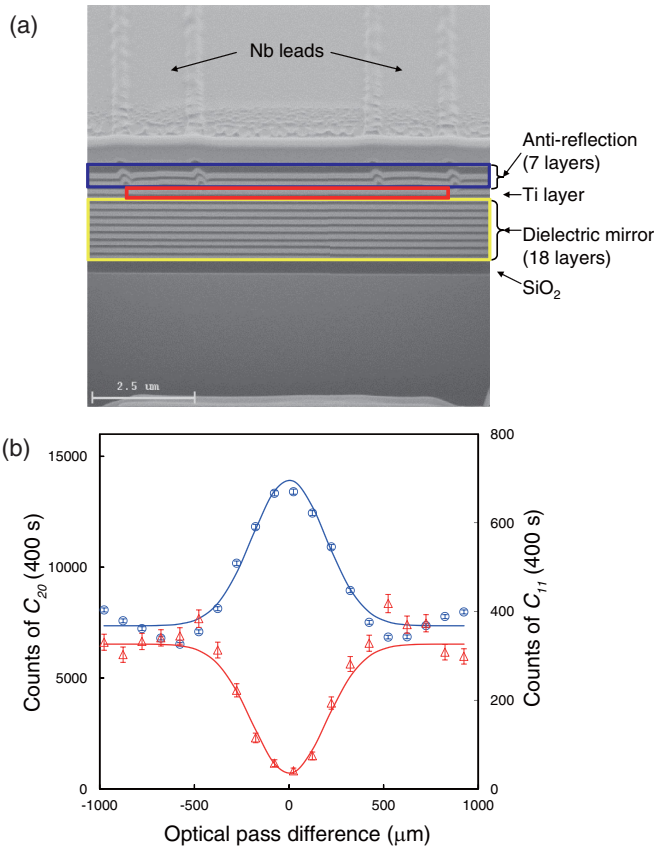

FIG. 2. (Color online) (a) Cross-sectional image of our TES. The layers highlighted by the yellow, red, and blue boxes are the dielectric mirror, Ti layer, and antireflection coating, respectively. (b) Counts of C_{20} (blue circle) and C_{11} (red triangle) in the two-photon interference using a 50/50 optical splitter as a function of the optical path difference. The best-fit curves of C_{20} (blue line) and C_{11} (red line) are derived from Eq. (2).

one would be due to the interaction of the modes in the bending region [16]. The mode-interaction length in the bending region of our LRSPP-DC was found to be 0.4 mm, while that of the LRSPP-DC in Ref. [16] was 0.7 mm, which makes T smaller than R of our LRSPP-DC.

III. PHOTON-NUMBER-RESOLVING DETECTOR BASED ON A SUPERCONDUCTING TRANSITION EDGE SENSOR

The visibility of the quantum interference of single SPPs is given by the following expression [19,20]:

$$V = \frac{2RT}{R^2 + T^2} I, \tag{1}$$

where I is the indistinguishability of single SPPs. Assuming that I is unity, V is expected to be 0.91.

In order to demonstrate the quantum interference of single SPPs using the LRSPP-DC with the high insertion loss, extremely sensitive and high-speed single-photon detection is required. We employed a photon-number-resolving detector based on using a 50/50 optical splitter and a superconducting transition edge sensor (TES). At telecommunication wavelengths, our TES has achieved the highest detection efficiency and the lowest dark count rate (R_D) among the existing single-photon detectors [21] Figure 2(a) shows a cross-sectional image of our TES. A titanium film was sandwiched between the antireflection coating and the dielectric mirror to maximize the detection efficiency. The maximum single-photon detection efficiency was 84% and the photon-number resolution was 0.38 at a wavelength of 1550 nm. Moreover, the response time of 100 ns and the timing jitter of 30 ns enabled us to detect single photons in the MHz region [22].

Using the photon-number-resolving detectors, we can observe the two-photon interference by measuring the coincidence between two-photon detection and zero-photon detection (C_{20}) or the coincidence between one-photon detection and one-photon detection (C_{11}). The signal-to-noise ratio (SNR) in the coincidence measurements can be evaluated using a coincidence to accidental coincidence ratio (CAR) [23]. The accidental count in C_{20} is much lower than that in C_{11} when both coincidence rates are the same [24], because the R_D due to the black-body radiation decreases as the number of photons to detect increases. Therefore, the measurement of C_{20} has a great advantage in SNR.

We observed the two-photon interference by measuring both C_{20} and C_{11} in a HOM interference experiment using a 50/50 optical splitter [25]. Figure 2(b) shows C_{20} and C_{11} as a function of the optical path difference. We can clearly see a dip in C_{11} and a bump in C_{20} when the optical path difference is zero, which indicates that photons are bunched by the bosonic quantum interference. The photon bunching is directly demonstrated by the bump in C_{20} and indirectly by the dip in C_{11}. Here we set the discrimination levels in the

measurements of C_{20} and C_{11} so that C_{20} has the same CAR as C_{11}. Then the two-photon detection efficiency was 64% with the R_D of 0.05 Hz and the one-photon detection efficiency was 20% with the R_D of 10 Hz. Note that the count of C_{20} was approximately 23 times higher than that of C_{11}. Therefore, we measured C_{20} to demonstrate the quantum interference of single SPPs through overcoming the high insertion loss of the LRSPP-DC.

IV. EXPERIMENT

The experimental setup for demonstrating the quantum interference of single SPPs is depicted in Fig. 3. A photon pair (signal and idler photons) at a wavelength of 1551 nm is generated through a spontaneous parametric down-conversion process (SPDC) in a 6-mm-long type-II periodically poled lithium niobate (PPLN) pumped by an external cavity diode laser at a wavelength of 775.5 nm. The signal and idler photons were separated by a polarizing beam splitter (PBS), and subsequently coupled into the polarization maintaining fibers (PMFs). To control the polarization of photons, half-wave plates (HWPs) were inserted between the PBS and the PMFs. The excited single SPPs were superposed in the interaction region of the LRSPP-DC and finally converted into single photons at the end facets. The single photons were subsequently coupled to the single mode fibers (SMFs) and led to TESs. Here, to reduce the degradation of the indistinguishability between signal and idler photons due to the dispersion in the PPLN [26], the wave packets of the photons were expanded using narrow band-pass filters (NBPFs) with a bandwidth of 4.2 nm (which is much narrower than the bandwidth of the photon pairs, ~25 nm) [8]. In addition, noise photons with high energy emitted from the measuring instruments were eliminated using fiber-based band-pass filters (FBPFs). The output signals from TESs were led to the discriminators (DISC1, 2). Finally, the anticoincidence between the outputs from DISC1 and 2, which corresponds to the coincidence

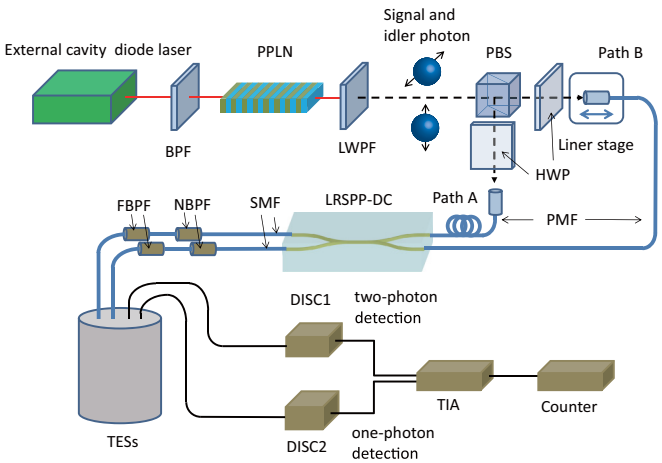

FIG. 3. (Color online) Experimental setup. BPF, band-pass filter; LWPF, long-wavelength pass filter; PBS, polarizing beam splitter; HWP, half-wave plate; PMF, polarization maintaining fiber; SMF, single mode fiber; NBPF, narrow band-pass filter; FBPF, fiber based band-pass filter; TESs, superconducting transition edge sensors; DISC, discriminator; TIA, time interval analyzer.

between two-photon detection and zero-photon detection, was measured using a time interval analyzer (TIA) and a counter.

V. RESULTS AND DISCUSSION

First, we investigated the indistinguishability between signal and idler photons and their bandwidths using a 50/50 optical splitter instead of the LRSPP-DC in Fig. 3. The measured coincidence counts shown in Fig. 2(b) were fitted to the following equation [9,25]:

$$N_C^{\pm} = C^{\pm}[1 \pm V \exp(-\Delta\omega^2\delta\tau^2)] + C_{\mathrm{TA}}^{\pm}, \tag{2}$$

where $\Delta\omega$ is a bandwidth of photon pairs, $\delta\tau$ is an optical path difference, V is a visibility given by Eq. (1), $C^{\pm}$ is a constant, and $C_{\mathrm{TA}}^{\pm}$ is a total accidental coincidence count. The plus (minus) sign denotes the count of C_{20} (C_{11}). The total accidental coincidence count between one-photon detection and one-photon detection C_{TA}^{-} was evaluated simply by counting the coincidence setting the optical pass difference much longer than the coherence length of the signal and idler photons. On the other hand, the total accidental coincidence count between two-photon detection and zero-photon detection C_{TA}^{+} (i.e., spurious two-photon detections) can be expressed by the following equation:

$$C_{\mathrm{TA}}^{+} = C_{\mathrm{multi}} + C_{\mathrm{black}} + C_{\mathrm{noise}} + C_{\mathrm{visible}}, \tag{3}$$

where C_{multi} denotes two-photon detections caused by the photons from different pairs in the coincidence time window, C_{black} denotes two-photon detections including photons at a wavelength of 2000 nm due to black-body radiation, C_{noise} denotes spurious two-photon detections caused by the TES noise including the Johnson noise, phonon noise, and readout noise [27] that was superposed on the one-photon detection signal, and C_{visible} denotes detections of a visible photon originated from measuring instruments. Since the energy of the visible single photon is more than that of two photons at a wavelength of 1550 nm, the detection of the visible single photon causes a spurious two-photon detection. Since C_{visible} is not caused by the photons generated through a SPDC process, it can be measured by blocking both input ports of path A and B. The sum of C_{multi}, C_{black}, and C_{noise} caused by the photons through the path A (B) plus C_{visible} can be measured by blocking input port of path B (A). Here we denote the coincidence count measured blocking input port B (A) by C_{A} (C_{B}). Therefore, Eq. (3) can be rewritten as the following equation:

$$C_{\mathrm{TA}}^{+} = C_{\mathrm{A}} + C_{\mathrm{B}} - C_{\mathrm{visible}}. \tag{4}$$

C_{TA}^{+} was calculated using the measured C_{A}, C_{B}, and C_{visible}.

According to the regression analysis using Eq. (2), the two-photon interference visibility and the bandwidth of single photons were 98.7 ± 3.2% and 0.95 ± 0.04 THz, respectively. Since the optical directional coupler has approximately a 50/50 output ratio, the indistinguishability of signal and idler photons is equals to the visibility [see Eq. (1)].

Next, we measured the anticoincidence C_{20} replacing the 50/50 optical splitter with the LRSPP-DC to directly demonstrate the photon bunching due to the quantum interference of SPPs. Figure 4 shows the anticoincidence counts as a

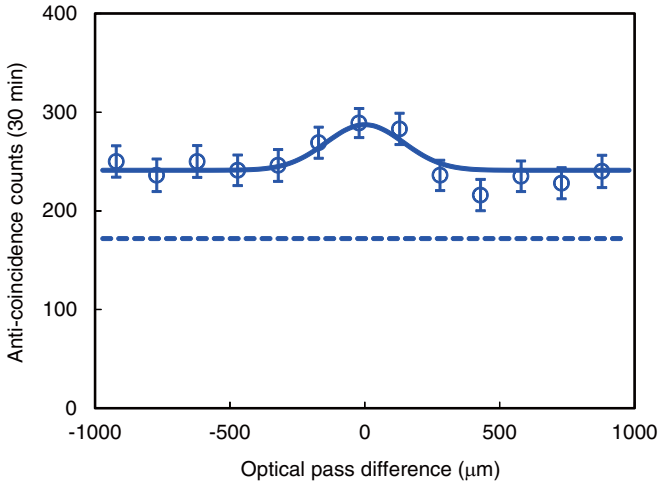

FIG. 4. (Color online) Anticoincidence counts between two-photon detection and one-photon detection as a function of the optical path difference. The best-fit curve (solid line) is derived from Eq. (2). The estimated total accidental coincidence count (dashed line) is also shown.

function of the optical path difference. Since a single SPP is converted into a single photon at the end facets of the LRSPP-DC [7], the photon bunching is the evidence that the quantum interference of single SPPs is bosonic. The calculated $C^{\pm}$ from the measured coincidence counts was 172 counts. According to the regression analysis using Eq. (2) with the plus sign, the two-SPP interference visibility and the bandwidth of single SPPs were 84.3 ± 9.1% and 0.80 ± 0.18 THz, respectively. Hence the indistinguishability of single SPPs was estimated to be 92.6% from Eq. (1). This result indicates that the indistinguishability of photons to excite SPPs is well preserved in the process of photon-SPP mode conversion. The bandwidth of single SPPs was in agreement with the bandwidth of single photons within the error.

VI. CONCLUSIONS

We have experimentally demonstrated the quantum interference of single LRSPPs. The photon bunching with the interference visibility of 84.3% was observed when the quantum interference of single SPPs occurred, which is the clear evidence that SPPs are bosonic quantum particles. Additionally, we have demonstrated that the indistinguishability of photons that excite single SPPs is well preserved in the process of photon-SPP mode conversion. These results suggest the feasibility of the QIP using a plasmonic circuitry based on LRSPP-WGs. Although our LRSPP-WGs have micronsize widths, replacing them with nanosized LRSPP-WGs, e.g., multilayer metal-dielectric planar waveguides [28] whose widths are submicron and field confinements are as small as those of short-range SPP waveguides, we can easily scale down our plasmonic circuitry. Moreover, the huge insertion losses of our LRSPP-DC would be improved significantly using such waveguides. The nanosized circuitry would have an advantage to scale up the quantum simulation of boson sampling that has recently been demonstrated using silicon photonic waveguides [29].

ACKNOWLEDGMENTS

The authors would like to thank S. Mori and N. Namekata for valuable discussions. A part of this work was conducted at the Nano-Processing Facility, supported by IBEC innovation Platform, AIST.

[1] Fitrilawati, R. E. Siregar, and M. O. Tjia, J. Mat. Sains **2**, 16 (1997); W. L. Barnes, A. Dereux, and T. W. Ebbesen, Nature (London) **424**, 824 (2003).
[2] S. Kim, J. Jin, Y. J. Kim, I. Y. Park, Y. Kim, and S. W. Kim, Nature (London) **453**, 757 (2008).
[3] A. V. Akimov, A. Mukherjee, C. L. Yu, D. E. Chan, A. S. Zibrov, P. R. Hemmer, H. Park, and M. D. Lukin, Nature (London) **450**, 402 (2007).
[4] R. Kolesov, B. Grotz, G. Balasubramanian, R. J. Stöhr, A. A. L. Nicolet, P. R. Hemmer, F. Jelezko, and J. Wrachtrup, Nat. Phys. **5**, 470 (2009).
[5] M. S. Tame, K. R. McEnery, S. K. Ozdemir, J. Lee, S. A. Maier, and M. S. Kim, Nat. Phys. **9**, 329 (2013).
[6] E. Altewischer, M. P. van Exter, and J. P. Woerdman, Nature (London) **418**, 304 (2002); S. Fasel, F. Robin, E. Moreno, D. Erni, N. Gisin, and H. Zbinden, Phys. Rev. Lett. **94**, 110501 (2005); A. Huck, S. Smolka, P. Lodahl, A. S. Sørensen, A. Boltasseva, J. Janousek, and U. L. Andersen, *ibid.* **102**, 246802 (2009); R. W. Heeres, S. N. Dorenbos, B. Koene, G. S. Solomon, L. P. Kouwenhoven, and V. Zwiller, Nano Lett. **10**, 661 (2010).
[7] G. Di Martino, Y. Sonnefraud, S. Kéna-Cohen, M. Tame, Ş. K. Özdemir, M. S. Kim, and S. A. Maier, Nano Lett. **12**, 2504 (2012).
[8] G. Fujii, T. Segawa, S. Mori, N. Namekata, D. Fukuda, and S. Inoue, Opt. Lett. **37**, 1535 (2012).
[9] C. K. Hong, Z. Y. Ou, and L. Mandel, Phys. Rev. Lett. **59**, 2044 (1987).
[10] R. W. Heeres, L. P. Kouwenhoven, and V. Zwiller, Nat. Nanotechnol. **8**, 719 (2013).
[11] R. Ghosh and L. Mandel, Phys. Rev. Lett. **59**, 1903 (1987).
[12] R. Charbonneau, N. Lahoud, G. Mattiussi, and P. Berini, Opt. Express **13**, 977 (2005).
[13] B. Cabrera, R. M. Clarke, P. Colling, A. J. Miller, and S. Nam, Appl. Phys. Lett. **73**, 735 (1998).
[14] J. T. Kim, S. Park, J. J. Ju, S. K. Park, M.-S. Kim, and M.-H. Lee, IEEE Photon. Technol. Lett. **19**, 1374 (2007).
[15] T. Nikolajsen, K. Leosson, I. Salakhutinv, and S. I. Bozhevolnyi, Appl. Phys. Lett. **82**, 668 (2003).
[16] A. Botlasseva and I. S. Bozhevolnyi, IEEE J. Sel. Top. Quant. Electron. **12**, 1233 (2006).
[17] R. Charbonneau, C. Scales, I. Breukelaar, S. Fafard, N. Lahoud, G. Mattiussi, and P. Berini, J. Lightwave Technol. **24**, 477 (2006).
[18] G. I. Stegeman, R. F. Wallis, and A. A. Maradudin, Opt. Lett. **8**, 386 (1983).

[19] M. Tanida, R. Okamoto, and S. Takeuchi, Opt. Express **20**, 15275 (2012).
[20] P. J. Thomas, J. Y. Cheung, C. J. Chunnilall, and M. H. Dunn, Appl. Opt. **49**, 2173 (2010).
[21] M. D. Eisaman, J. Fan, A. Migdall, and S. V. Polyakov, Rev. Sci. Instrum. **82**, 071101 (2011).
[22] D. Fukuda, G. Fujii, T. Numata, A. Yoshizawa, H. Tsuchida, H. Fujino, H. Ishii, T. Itatani, S. Inoue, and T. Zama, Metrologia **46**, S288 (2009).
[23] H. Takesue and K. Inoue, Opt. Express **13**, 7832 (2005).
[24] N. Namekata, Y. Takahashi, G. Fujii, D. Fukuda, S. Kurimura, and S. Inoue, Nat. Photon. **4**, 655 (2010).
[25] G. Di Giuseppe, M. Atatüre, M. D. Shaw, A. V. Sergienko, B. E. A. Saleh, M. C. Teich, A. J. Miller, S. W. Nam, and J. Martinis, Phys. Rev. A **68**, 063817 (2003).
[26] G. Fujii, N. Namekata, M. Motoya, S. Kurimura, and S. Inoue, Opt. Express **15**, 12769 (2007).
[27] K. D. Irwin, Appl. Phys. Lett. **66**, 1998 (1995).
[28] Y. Bian and Q. Gong, J. Opt. **16**, 015001 (2014).
[29] J. B. Spring, B. J. Metcalf, P. C. Humphreys, W. S. Kolthammer, X.-M. Jin, M. Barbieri, A. Datta, N. T. Peter, N. K. Langford, D. Kundys, J. C. Gates, B. J. Smith, P. G. R. Smith, and I. A. Walmsley, Science **339**, 798 (2013).